ELSEVIER

Polymer 43 (2002) 3691–3698

polymer

www.elsevier.com/locate/polymer

Effect of supercritical CO_2 on phase structure of PEO/PVAc blends evaluated from SAXS absolute intensity measurement

Yeong-Tarng Shieh[a,*], Yen-Gu Lin[a], Hsin-Lung Chen[b]

[a]*Department of Chemical Engineering, National Yunlin University of Science and Technology, 123 University Road, Section 3, Touliu, Yunlin 640, Taiwan, ROC*

[b]*Department of Chemical Engineering, National Tsing Hua University, Hsin-Chu 300, Taiwan, ROC*

Received 11 December 2001; received in revised form 25 February 2002; accepted 27 February 2002

Abstract

The effect of supercritical CO_2 on the morphological structure of crystalline/amorphous PEO/PVAc blends was investigated by means of SAXS with the measurement of absolute scattering intensity. The morphological structure of PEO/PVAc exhibited a considerable change upon CO_2 treatment as demonstrated by the drastic increase of scattering intensity, or the enhancement of electron density contrast between the crystalline and amorphous layers in the lamellar stacks, resulting from the swelling of amorphous PEO via the incorporation of CO_2 into the interlamellar (IL) regions and/or the expulsion of PVAc from the IL regions. Upon CO_2 treatment, the crystal and amorphous layer thickness (l_c and l_a, respectively) were both increased. Compared with the increase of l_a, the increase of l_c was relatively significant and was attributed to the occurrence of melting and recrystallization during CO_2 treatment leading to thicker PEO crystals via a depression of equilibrium melting temperature and/or an increase of crystal fold surface free energy. The measured electron density contrast revealed that the distance of segregation in PEO/PVAc blends involved the extralamellar segregation before CO_2 treatments and the swelling of interlamellar region dominated the drastic increase of scattering intensity after CO_2 treatments. The finding of extralamellar morphology was consistent with the magnitude of volume fraction of lamellar stacks in the blends. The lamellar size distribution appeared to be broader and the lamellar stacks more disorganized for the blends after CO_2 treatments according to SAXS one-dimensional correlation function profiles.

Keywords: Crystallization; Phase segregation; Lamellar

1. Introduction

Crystallization of a melt-miscible crystalline/amorphous blend involves the segregation of amorphous diluent. Depending upon the distance of segregation, various types of morphology may be created. These segregation types include (1) interlamellar (IL) segregation, where segregation of the diluent occurs at lamellar level, so that the diluent is located in the IL regions; (2) interfibrillar (IF) segregation, where the diluent is segregated by a larger distance to the regions between the lamellar bundles in spherulites; and (3) interspherulitic (IS) segregation, where the diluent is segregated by the largest distance to the regions between spherulites [1,2]. The latter two types characterized by the longer segregation distance are also termed as 'extralamellar segregations'. These morphological patterns represent the diluent dispersion from nanoscopic scale for IL segregation to micrometer scale for IS segregation. Different scales of segregation may lead to different properties. A blend system does not necessarily exhibit only one type of morphology. Different types of morphology may coexist leading to multiple locations for the amorphous diluent [3–7].

Keith and Padden [8] suggested that the distance over which uncrystallizable diluent may be segregated is determined by the interplay between the diffusion coefficient (D) of impurity molecules and the crystal growth rate (G). If the diffusion of diluent is relatively slow compared to the crystal growth, the diluent molecules may be trapped inside the IL regions. If diluent diffusion is faster, on the other hand, extralamellar segregation is generated. The interplay between D and G is defined by the parameter, $\delta = D/G$. δ has the unit of length and thus provides a qualitative measure of segregation distance. δ may depend on the composition, temperature, molecular weight, and polymer–polymer interaction of the blend.

Poly(ethylene oxide) (PEO)/poly(vinyl acetate) (PVAc)

* Corresponding author. Tel.: +886-5-534-2601; fax: +886-5-531-2071.
E-mail address: shiehy@pine.yuntech.edu.tw (Y.-T. Shieh).

0032-3861/02/$ - see front matter
PII: S0032-3861(02)00190-8

crystalline/amorphous blends have been known to be compatible by both theoretical prediction and experimental results [9–16]. Segregation morphology of PEO/PVAc blends has been studied. Martuscelli and Silvestre and coworkers [11,12] examined the segregation morphology by small angle X-ray scattering (SAXS) and found that PVAc was incorporated into the IL regions of PEO crystals. Segregation of the amorphous diluent was found to strongly depend on T_g and molecular weight [17]. Runt and coworkers [18] found that segregation of the weakly interacting polymer pairs (e.g. PEO/poly(methyl methacrylate) (PMMA) and PEO/PVAc) was largely dependent on glass transition temperatures (T_g) of the amorphous diluent. The high-T_g diluent (e.g. PMMA) was found to reside exclusively in IL regions whereas the low-T_g diluent (e.g. PVAc) was excluded at least partially into IF regions. The introduction of strong intermolecular interactions between the crystallizable and amorphous components resulted in significantly reduced crystal growth rates and promoted diluent segregation over greater length scales, regardless of diluent mobility at the crystallization temperature. Although diluent mobility contributed to diluent segregation, the growth of the PEO crystals, and the factors that influenced the growth rate, dominated the length scale of diluent segregation.

SAXS has been a powerful tool for probing the detailed microstructure of crystalline/amorphous blends in our previous reports [19–24]. The morphological parameters in the lamellar level such as the long period (L), crystal layer thickness (l_c), and amorphous layer thickness (l_a) can be deduced from the one-dimensional correlation function or the interphase distribution function. Close examination on the composition variation of l_a may reveal the existence of IL segregation [25–27]. The volume fraction of lamellar stacks (ϕ_s) given by the ratio of volume fraction of bulk crystallinity (ϕ_c) to the volume fractional crystallinity within the lamellar stacks (ϕ_{cs}), i.e. $\phi_s = \phi_c/\phi_{cs}$, could serve as a measure for the extent of IL segregation [24]. When the absolute scattering intensity is available, the perturbation of intensity upon blending or treatment may be connected with the change of phase structure of crystalline/amorphous blends.

Supercritical CO_2 fluids or compressed CO_2 gases or liquids have recently drawn much attention because the environmentally friendly CO_2 (especially the supercritical state CO_2) is a potential candidate to be an alternative to substitute for organic chemicals used in modification and processing of polymers, such as being used as a foaming agent to prepare microcellular foams [28–31], a processing aid to reduce melt viscosity in injection molding [32–35], a nucleating agent to induce crystallization [36–38]. Upon treatment of the supercritical fluids, the phase structure of polymers may be perturbed and hence the properties could be modified accordingly; it is thus important to reveal the effect of supercritical CO_2 on the phase structure of a polymer before the supercritical CO_2 can be practically used in applications of the polymer. In the present study, we probe the morphological structure of crystalline/amorphous PEO/PVAc blends treated by supercritical CO_2 by means of SAXS. It will be seen that the morphological structure of PEO/PVAc exhibits a significant change upon CO_2 treatment as demonstrated from the drastic perturbation of scattering intensity. In addition, with the absolute intensity, the electron density contrast between the crystalline and amorphous layers in the lamellar stacks can be evaluated very conveniently from the simple geometric analysis of the correlation function proposed by Strobl and Schneider [39]. The measured electron density contrast will be used to investigate the effect of supercritical CO_2 on the phase structure of crystalline/amorphous PEO/PVAc blends.

2. Experimental section

2.1. Materials and sample preparations

PEO with $M_v = 900,000$ was acquired from Aldrich Chemical Company (Milwaukee, WI) and PVAc with $M_w = 104,000$ and $M_w/M_n = 2.0$ was obtained from Chang Chun Plastics Corporation (Taipei, Taiwan). Uniform film samples of neat PEO or its blends with PVAc were prepared by dissolving 0.2 g neat PEO or the blends in 15 ml chloroform, followed by casting and drying at room temperature for 2 days. Specimens for CO_2 treatments were ca. 0.3 mm thick.

2.2. CO_2 Treatments

The CO_2 treatments were performed in a supercritical extractor supplied by ISCO (Lincoln, Nebraska) with a model SFX 2–10 which was equipped with a syringe pump with a model 260D. The polymer films for the CO_2 treatments were put in a 10 cm^3 cell located inside the extractor pressurized by the equipped syringe-type pump at 5000 psi and controlled at 32 °C. The treatment time was 1 h. A preliminary test showed that 1 h of treatment time was able to reach the equilibrium solubility of CO_2 in the film sample. After the treatment, the cell was depressurized to ambient pressure in less than 20 s. The sample after the CO_2 treatment showed a negligible weight change, indicating that neither CO_2 resided inside the film sample nor any part of the sample was dissolved away. The uniform PEO and PEO/PVAc films looked translucent and colorless before CO_2 treatments but turned into an opaque, milk white, collapsed film upon CO_2 treatments. The change in film appearance indicated that the melting and recrystallization of PEO had occurred upon CO_2 treatments.

2.3. Bulk crystallinity measurements

Volume fraction of bulk crystallinities (ϕ_c) of semicrystalline PEO/PVAc were calculated from mass fraction of bulk crystallinity (ω_c) which was determined by dividing

the heat of fusion of a sample by the heat of fusion of perfectly crystalline PEO. The heat of fusion in J/g of a sample was measured by a differential scanning calorimeter (DSC 2010) of TA Instruments (New Castle, DE). The heat of fusion of perfectly crystalline PEO is 205 J/g [40].

2.4. SAXS measurements

All SAXS measurements were performed at room temperature. The X-ray source was operated at 200 mA and 40 kV and was generated by a 18 kW rotating anode X-ray generator (Rigaku) with a rotating anode Cu target. The incident X-ray beam was monochromated by pyrolytic graphite and a set of three pinhole inherent collimators was used so that the smearing effects inherent in slit-collimated small-angle X-ray cameras can be avoided. The sizes of the first and second pinhole are 1.5 and 1.0 mm, respectively, and the size of the guard pinhole before the sample is 2.0 mm. The scattered intensity was detected by a two-dimensional position sensitive detector (Ordela Model 2201X, Oak Ridge Detector Laboratory Inc.) with 256×256 channels (active area 20×20 cm^2 with $\sim$1 mm resolution). The sample to detector distance is 4000 mm long. The beam stop is around lead disk of 18 mm in diameter. All data were corrected by the background (dark current and empty beam scattering) and the sensitivity of each pixel of the area detector. The area scattering pattern has been radially averaged to increase the efficiency of data collection compared with one-dimensional linear detector. Data were acquired and processed on an IBM-compatible personal computer.

3. Results and discussion

From DSC measurements for T_g of the PEO/PVAc blends prepared by solution casting from chloroform, a single composition-dependent T_g is identified over the entire composition range, indicating that PEO is miscible with PVAc in the amorphous region. The T_g of the blend is between those of pure PEO and PVAc being -65 and 32 °C, respectively, and increases with increasing PVAc content. The composition variation of T_g of the PEO/PVAc blends suggests that the amorphous regions of the blends are rubbery at the 32 °C of CO_2 treatment temperature in this study.

Fig. 1 shows the Lorentz-corrected SAXS profiles of neat PEO and its blends with PVAc prior to supercritical CO_2 treatments. The scattering intensity decreases with increasing incorporation of PVAc due to decreasing electron density contrast ($\Delta\eta = \eta_c - \eta_a$) between the crystalline and amorphous layers. The electron densities of crystalline PEO, amorphous PEO, and PVAc calculated from their mass densities (1.24, 1.12, and 1.19 g/cm^3, respectively) are 0.676, 0.612, and 0.636 mol/cm^3, respectively. The scattering intensity contrast decreases with increasing PVAc content, suggesting that the electron density of the IL regions is increased due to incorporation of PVAc into IL regions, as this would decrease the electron density contrast between the crystalline and amorphous layers. A second-order peak near $q = 0.32$ nm^{-1} can be roughly identified, indicating that a fairly well lamellar stacking in the samples.

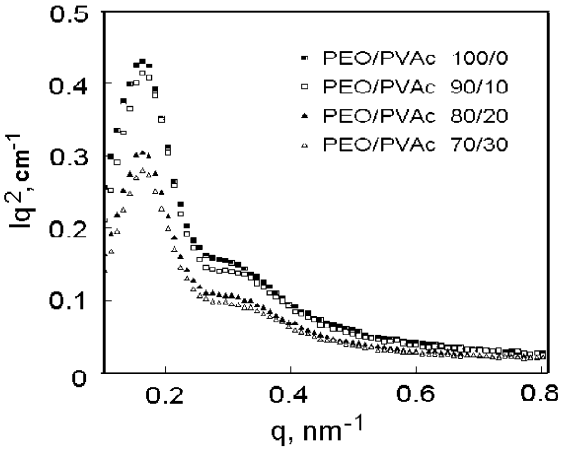

Fig. 1. Lorentz-corrected SAXS profiles of neat PEO and its blends with various amount of PVAc before CO_2 treatments.

Fig. 2 compares the Lorentz-corrected SAXS profiles of the samples between before and after supercritical CO_2 treatments. Neat PEO and the blends after CO_2 treatments

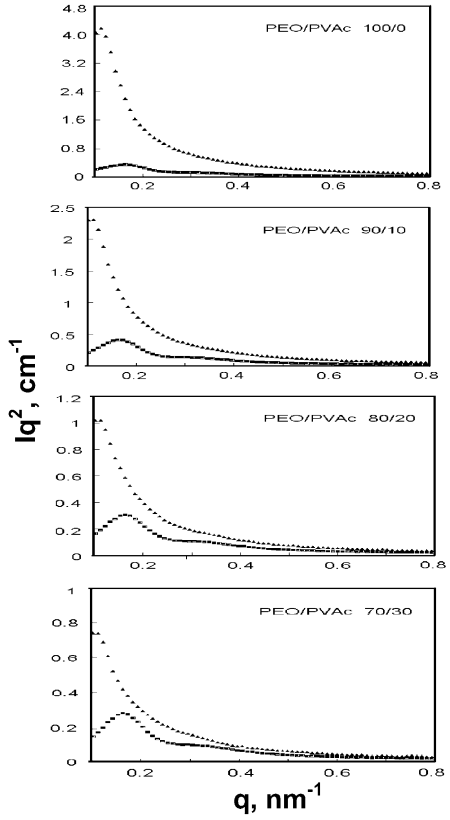

Fig. 2. Lorentz-corrected SAXS profiles of PEO/PVAc = 100/0, 90/10, 80/20, and 70/30. In each graph, rectangular and triangular symbols stand for samples for before and after CO_2 treatments, respectively.

apparently show much stronger scattering intensity than those before CO_2 treatments due to an increased electron density contrast between the crystalline and amorphous layers caused by the supercritical CO_2. For neat PEO the scattering intensity is increased upon CO_2 treatment suggesting that the electron density of amorphous PEO in the IL regions is decreased due to decreasing mass density through the swelling by CO_2, as this would increase the electron density contrast between the crystalline and amorphous layers. This suggestion is based on the observation of appearance of the sample changing from a uniform, translucent, and colorless film to a collapsed, opaque, and milk white film upon CO_2 treatments due to the presence of voids in the CO_2 treated sample. These voids include big and small ones. Big voids existing outside the lamellar stacks are apparently responsible for the milk white appearance for samples whereas small voids existing in the IL regions are responsible for the drastic increase of SAXS intensity and would disorganize the lamellar stacks as will be demonstrated later by the one-dimensional correlation function profiles in Fig. 7. For the blends upon CO_2 treatment, the enhanced scattering intensity may be somewhat due to the expulsion of PVAc from the IL regions in addition to the swelling effect as described earlier, since the electron density of PVAc is higher than that of amorphous PEO and hence the expulsion of PVAc from IL regions would increase the electron density contrast between the crystalline and amorphous layers of the lamellar stacks. The inference of the expulsion of PVAc from IL regions is based on infrared spectroscopy evidence that the carbonyl groups in PVAc exhibit specific interactions with CO_2 of Lewis acid-base nature [41]. These interactions might give rise to the expulsion of PVAc from IL regions during depressurizing of CO_2.

The weight-average long period associated with the lamellar stacks can be calculated from the peak maximum of the Lorentz-corrected SAXS profiles using the Bragg's equation, $L = 2\pi/q_{max}$. Fig. 3 shows the composition variation of long period for the blends before and after CO_2 treatments. The long periods of neat PEO and the blends before CO_2 treatments exhibit a roughly constant value at near 39 nm with an insignificant composition dependence. The long periods for samples after CO_2 treatments exhibit a significantly increased long period falling in the range 56–62 nm depending on the blend composition. In the lamellar stack model with sharp phase boundary, the long period represents the sum of the crystal thickness (l_c) and the amorphous layer thickness (l_a). Rise in long period may thus stem from the thickening of crystal layer or the swelling of amorphous layer. Two approaches may be utilized to determine the average thickness of the two layers, namely, the one-dimensional correlation function and the interphase distribution function. The one-dimensional correlation function was utilized to deconvolute long period into the thickness of these two types of layers. The correlation function, $K(z)$, defined by Strobl and Schneider, adopts the following form [39]:

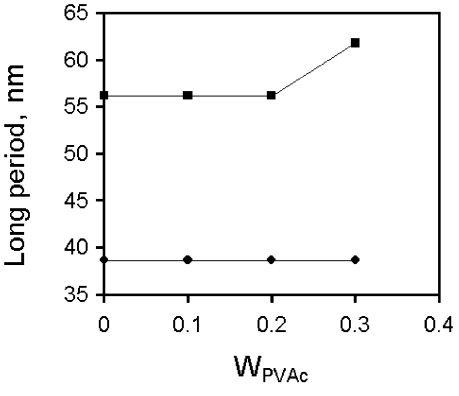

Fig. 3. Composition variation of long period of semicrystalline PEO/PVAc. Filled circle (●) and filled square (■) stand for samples for before and after CO_2 treatments, respectively.

$$K(z) = \frac{1}{2\pi^2}\int_0^\infty I(q)q^2\cos(qz)\mathrm{d}q \tag{1}$$

where $I(q)$ is the absolute scattering intensity obtained from the SAXS measurement, $q = 4\pi/\lambda\sin(\theta/2)$ (θ = scattering angle), and z is the direction along which the electron density is measured. $K(z)$ is different from the correlation function, $\gamma(z)$, defined by Vonk, where normalization by the invariant was introduced for $\gamma(z)$ [42,43].

Since the experimentally accessible q range is finite, extrapolation of intensity to both low and high q is necessary for the integrations. Extrapolation to zero q was accomplished by the Debye–Bueche model [44,45],

$$I(q) = \frac{A}{\left(1 + a_c^2q^2\right)^2} \tag{2}$$

where A is a constant and a_c is the correlation length. A and a_c can be determined from the plot of $I(q)^{-1/2}$ vs. q^2 using the intensity data at low q region. Extension to large q can be performed using the Porod–Ruland model [46],

$$I(q) = K_p\frac{\exp(-\delta^2q^2)}{q^4} + I_{fl} \tag{3}$$

where K_p is the Porod constant, δ is a parameter related to the thickness of crystal/amorphous interphase, and I_{fl} is the background intensity arising from thermal density fluctuation. The values of K_p, δ, and I_{fl} were obtained by curve fitting the intensity profile at high q region.

Fig. 4 shows the representative plot of $K(z)$. Assuming the corresponding two-phase model, l_c and l_a can be estimated via simple geometric analysis of $K(z)$. The thickness of the thinner layers (l_1) is given by the intersection between the straight line extended from the self-correlation triangle and the baseline given by $-A$. The average thickness of the thicker layer is then given by $l_2 = L - l_1$. The assignment of l_1 and l_2 is governed by the magnitude of the linear crystallinity within the lamellar stacks (ϕ_{cs}), where $\phi_{cs} = l_c/(l_c + l_a)$. When $\phi_{cs} < 0.5$, the crystals contribute to the

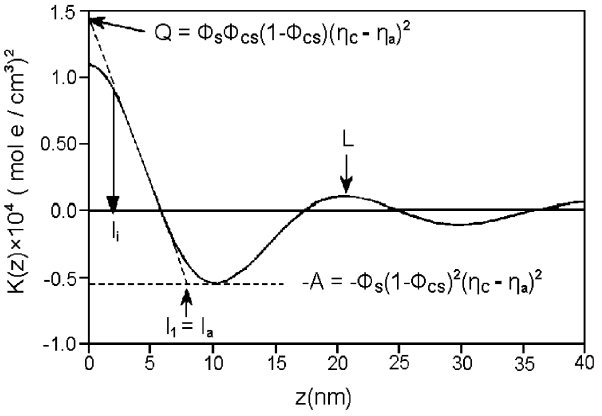

Fig. 4. Schematic plot of Strobl-Schneider's one-dimensional correlation function profile. Determinations of the lamellar layer thickness and the invariant assuming the corresponding two-phase model are demonstrated in the figure.

smaller thickness, thus $l_1 = l_c$ and $l_2 = l_a$. The inverse is true for $\phi_{cs} > 0.5$. ϕ_{cs} is related to the volume fraction of bulk crystallinity, ϕ_c, by

$$\phi_c = \phi_s \phi_{cs} \quad (4)$$

where ϕ_s is the volume fraction of lamellar stacks in the sample. Since $\phi_s \leq 1$, Eq. (4) prescribes that ϕ_c cannot be higher than ϕ_{cs}. As a result, the assignment of l_1 and l_2 would be rather straightforward for $\phi_c > 0.5$, because l_1 in this case must correspond to l_a and l_2 to l_c. From the DSC measurements, ϕ_c of neat PEO and the blends containing 10 and 20% PVAc lie above 0.5 (Table 1), l_1 and l_2 were thus assigned to l_a and l_c, respectively. l_a and l_c of these three samples before CO_2 treatment are thus near 7 and 32 nm, respectively, from the corresponding one-dimensional correlation function profiles (Fig. 5). Although ϕ_c of the blend containing 30% PVAc is below 0.5, l_1 can still be reasonably assigned to l_a and l_2 to l_c for this blend because a big difference between l_a and l_c is present for neat PEO and the blends containing 10 and 20% PVAc. This big difference between l_a and l_c is not likely to lead to an opposite assignment for l_a and l_c for the blend with ϕ_c below 0.5.

Fig. 6 shows plots of l_c and l_a as a function of the weight fraction of PVAc (W_{PVAc}). Like the long period, l_c and l_a of samples before CO_2 treatments are insignificantly varied with W_{PVAc}. The thickness of crystal layer (l_c) being weak

Table 1
The heats of fusion (ΔH, J/g), melting temperatures (T_m, °C), volume fractional bulk crystallinities (ϕ_c), and crystal layer thickness (l_C, nm) of PEO/PVAc blends for before and after CO_2 treatments

PEO/PVAc	Before CO_2 treatment				After CO_2 treatment			
	ΔH_1	T_{m1}	ϕ_{C1}	l_{C1}	ΔH_2	T_{m2}	ϕ_{C2}	l_{C2}
100/0	151.2	59.9	0.68	31.8	152.3	63.1	0.69	43.5
90/10	128.7	60.6	0.58	31.6	132.0	62.5	0.59	43.5
80/20	113.8	60.6	0.51	31.8	121.3	62.3	0.54	43.7
70/30	94.4	60.8	0.42	31.8	84.4	61.5	0.37	49.1

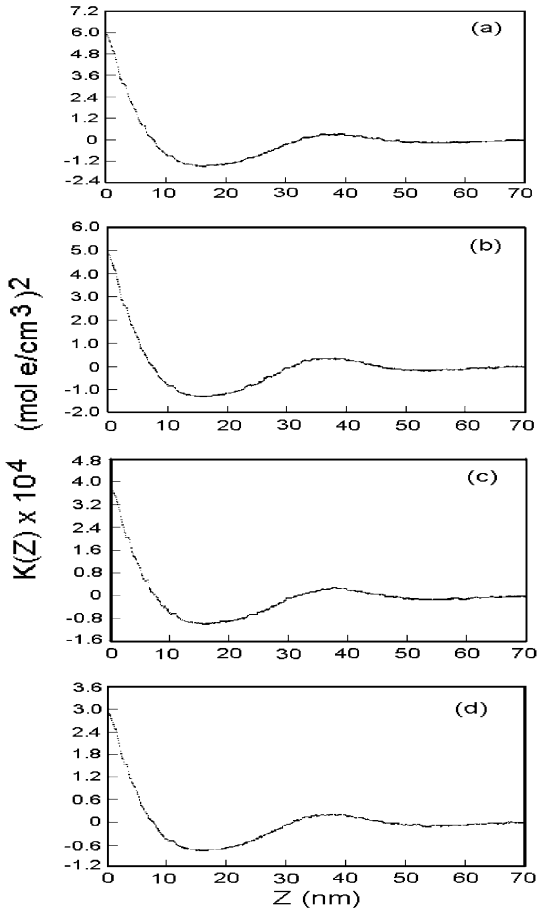

Fig. 5. One-dimensional correlation function of (a) neat PEO, (b) PEO/PVAc = 90/10, (c) PEO/PVAc = 80/20, (d) PEO/PVAc = 70/30 before CO_2 treatments.

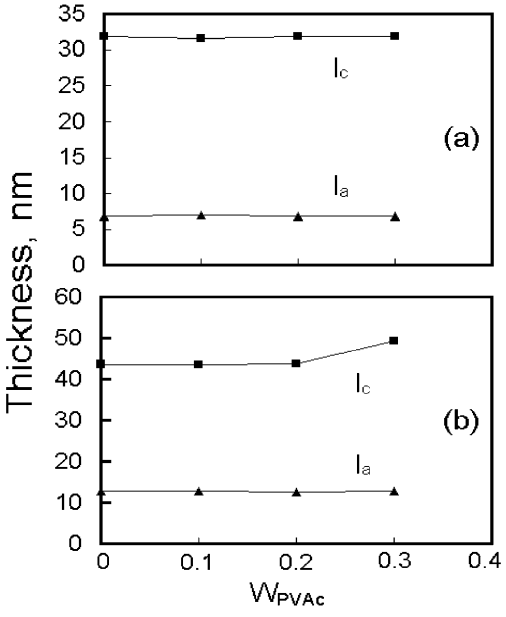

Fig. 6. Composition variations of l_c and l_a of PEO/PVAc for (a) before, and (b) after CO_2 treatments.

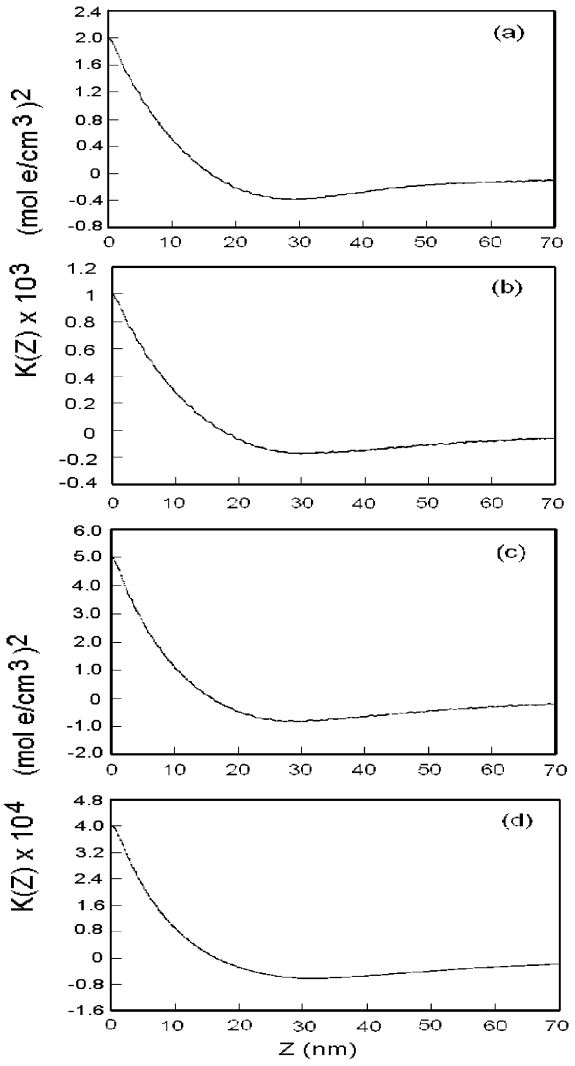

Fig. 7. One-dimensional correlation function of (a) neat PEO, (b) PEO/PVAc = 90/10, (c) PEO/PVAc = 80/20, (d) PEO/PVAc = 70/30 after CO_2 treatments.

functions of W_{PVAc} can be associated with the assumption of corresponding two-phase model in deriving l_c and l_a from $K(z)$, where the thickness of the crystal–amorphous interphase (l_i) is 'included' into the values of l_c and l_a. The interphase thickness can be estimated from the deviation from the self-correlation triangle near $z = 0$ (Figs. 4, 5 and 7). The values of l_i thus obtained are tabulated in Table 2. The interphase thickness for samples for both before and after CO_2 treatment appears to be <1 nm, which is much smaller than l_c or l_a. These small l_i values may be responsible for the observed weak functions of W_{PVAc} for l_c of samples before CO_2 treatment. The thickness of amorphous layer (l_a) being weak functions of W_{PVAc} before CO_2 treatment indicates that increasing PVAc does not swell the IL regions. This suggests that the increased PVAc content forms an extralamellar morphology. This result is not similar to what was obtained in Martuscelli and coworkers' work [11] having a finding of only IL morphology for the PEO/PVAc blends due to different sample preparations and/or molecular weight of PEO used between the previous work and this work. Samples used in the earlier work were subjected to heating and cooling treatments whereas samples studied in this work were prepared by solvent casting without being subjected to heating and cooling treatments. Moreover, according to Runt and coworkers' work [18], factors that would reduce crystal growth rates could promote diluent segregation over greater length scales regardless of the diluent mobility at the crystallization temperature. PEO used in this work has a very high molecular weight that might have a reduced crystal growth rate. It is thus not unreasonable that the extralamellar morphology is obtained in this work. Since the purpose of this work is to investigate the effect of CO_2 treatments on the phase structure of the blends, the disparity on the segregation morphology of the blends between the previous work and this work is not examined further here.

Table 2
Thickness of crystal-amorphous interphase (l_i) estimated from $K(z)$ of PEO/PVAc blends for before and after CO_2 treatments

PEO/PVAc	Before CO_2 treatment l_i (nm)	After CO_2 treatment l_i (nm)
100/0	0.73	0.98
90/10	0.73	0.98
80/20	0.91	0.98
70/30	0.91	0.98

Variation of l_a and l_c with PVAc composition for samples after CO_2 treatment is also displayed in Fig. 6. l_a and l_c of samples exhibit significant increases upon CO_2 treatment. After CO_2 treatment, the amorphous and crystal layer thickness of neat PEO is raised by about 6 and 12.6 nm, respectively, which are much larger than the magnitude of l_i. The swelling of l_a is attributed to the incorporation of CO_2 into the IL regions and thus the mass density is decreased, which is consistent with the enhancement of scattering intensity after CO_2 treatment observed in Fig. 2. The increased amorphous layer thickness upon CO_2 treatment exhibits an insignificant dependence on composition suggesting that the swelling of amorphous PEO in IL regions dominates the increase of the amorphous layer thickness.

The significant increase in l_c of neat PEO upon CO_2 treatment is associated with the occurrence of melting and recrystallization during CO_2 treatment that leads to thicker PEO crystals via a depression of equilibrium melting temperature and/or an increase of crystal fold surface free energy. It has been reported that the crystal fold surface free energy can be increased by CO_2 treatments for PET and sPS [47]. According to the secondary nucleation theory, the initial crystal thickness is given by [48,49]

$$l_g^* = \frac{2\sigma_e T_m^0}{\Delta h_f^0 (T_m^0 - T_c)} + \delta l \tag{5}$$

where σ_e is the fold surface free energy and Δh_f^0 is the bulk enthalpy of melting per unit volume. At low to moderate

degree of supercooling, δl is small. Eq. (5) thus reduces to

$$l_g^* \cong \frac{2\sigma_e T_m^0}{\Delta h_f^0 (T_m^0 - T_c)} \quad (6)$$

The final crystal thickness, according to the notation of Hoffman and Weeks [48,49], is γ times the initial thickness, i.e.

$$l_c = \gamma l_g^* \quad (7)$$

where γ is the so-called lamellar thickness factor. Eq. (6) prescribes that the initial crystal thickness is inversely proportional to the degree of supercooling. Thus, a depression of T_m^0 upon CO_2 treatment that would lower the degree of supercooling at a given T_C can lead to the formation of thicker crystals. As can be also known from Eq. (6), an increased crystal fold surface free energy during CO_2 treatment can also give rise to the increase of l_c. From Fig. 6(b), l_c increases with increasing W_{PVAc} due to the depression of equilibrium melting temperature of PEO upon blending with PVAc [11].

It is noted that the values of l_a and l_c determined from $K(z)$ could face a large uncertainty because the broad lamellar size distribution could shift the position of the baseline ($-A$) [39]. On the other hand, the electron density contrast, $\Delta\eta$, can be determined from $K(z)$ with better confidence in that $\Delta\eta$ is much less sensitive to the perturbation of baseline position for the samples with intermediate crystallinity ($0.3 < \phi_{cs} < 0.7$). As shown in Fig. 4, the invariant (Q) of the corresponding two-phase model for a sample (as in Figs. 5 and 7) is obtained by extrapolation from the self-correlation triangle to $z = 0$ [39]. The invariant is related to the electron density contrast by [39]

$$Q = \phi_s \phi_{cs} (1 - \phi_{cs}) \Delta\eta^2 \quad (8)$$

where ϕ_{cs} is the crystallinity within the lamellar stacks given by

$$\phi_{cs} = \frac{Q}{A + Q} \quad (9)$$

and ϕ_s is given by ϕ_c/ϕ_{cs} from Eq. (4). ϕ_c, as tabulated in Table 1, is volume fraction of bulk crystallinity and is calculated from weight fraction of crystallinity (ω_c) measured by DSC according to Eq. (10).

$$\phi_c = \frac{\dfrac{\omega_c}{\rho_c}}{\dfrac{\omega_c}{\rho_c} + \dfrac{(1 - \omega_c)}{\rho_a}} = \frac{\omega_c}{\omega_c + \dfrac{\rho_c}{\rho_a}(1 - \omega_c)} \quad (10)$$

The weight fraction of crystallinity (ω_c) is determined by dividing the heat of fusion, ΔH, in J/g of a sample by ΔH^0, which is 205 J/g for perfectly crystalline PEO [40]. ρ_c (1.24 g/cm^3) and ρ_a (ca 1.12 g/cm^3) are mass densities of crystal and amorphous component, respectively. $\Delta\eta$ can be calculated by Eq. (8) with the knowledge of Q, ϕ_{cs}, and ϕ_c. Table 3 tabulated the $\Delta\eta$ values obtained from the measured

Table 3
The measured $\Delta\eta$ ($= \eta_c - \eta_a$) values of PEO/PVAc blends for before ($\Delta\eta_{msd.1}$) and after ($\Delta\eta_{msd.2}$) CO_2 treatments

PEO/PVAc	$\Delta\eta_{msd.1}$	$\Delta\eta_{msd.2}$
100/0	0.071	0.112
90/10	0.070	0.086
80/20	0.069	0.069
70/30	0.068	0.075

invariant as a function of W_{PVAc} for both before and after CO_2 treatments. $\Delta\eta_{msd.1}$ and $\Delta\eta_{msd.2}$ are used to denote those measured $\Delta\eta$ values for before and after CO_2 treatments, respectively. The plots of $\Delta\eta_{msd.1}$ and $\Delta\eta_{msd.2}$ as a function of W_{PVAc} are shown in Fig. 8.

As can be seen in Table 3 and Fig. 8, the $\Delta\eta_{msd.1}$ is insignificantly varied with W_{PVAc} suggesting that the amount of incorporation of PVAc into IL regions does not increase with increasing W_{PVAc} and thus the distance of segregation in PEO/PVAc blends involves the extralamellar segregation. Comparing between $\Delta\eta_{msd.1}$ and $\Delta\eta_{msd.2}$ for neat PEO, the CO_2 treatment can cause an enhancement in electron density contrast resulting from the swelling of IL regions by CO_2. This enhancement decreases with increasing W_{PVAc} up to 0.2, indicating that below 0.2 W_{PVAc} the swelling of the IL regions by CO_2 decreases with increasing W_{PVAc}. The measured electron density contrast for the blend containing 30% PVAc is higher than that containing 20% PVAc, indicating that the expulsion of PVAc from IL regions has occurred upon CO_2 treatment. These results are supported by the observation of the composition variation of appearance of film samples after CO_2 treatments.

The presence of extralamellar morphology in the prepared blends can be demonstrated by the measured ϕ_s values of less than unity. Fig. 9 shows these measured ϕ_s values (ϕ_{s1} and ϕ_{s2} for before and after CO_2 treatments, respectively) plotting as a function of W_{PVAc}. As can be seen in Fig. 9, for neat PEO, the ϕ_{s1} is less than unity, suggesting that the extralamellar segregation of PEO forms before blending with PVAc. The ϕ_{s1} decreases with increasing W_{PVAc}, suggesting that the segregation distance increases with increasing W_{PVAc}. Upon CO_2 treatment, the

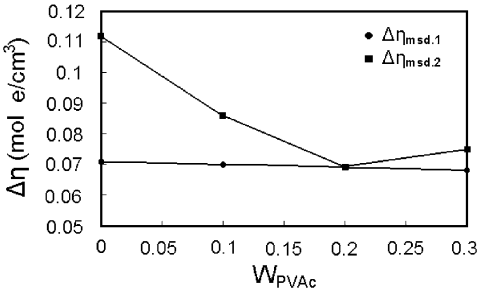

Fig. 8. Comparison between composition variation of the measured $\Delta\eta$ values for before ($\Delta\eta_{msd.1}$) and after ($\Delta\eta_{msd.2}$) CO_2 treatments.

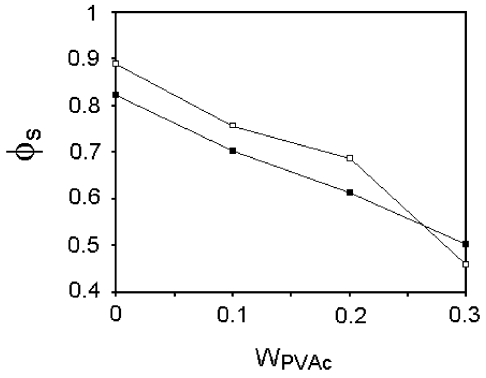

Fig. 9. Composition variation of the volume fraction of lamellar stacks (ϕ_s) for before (■) and after (□) CO_2 treatments.

segregation distance is decreased for neat PEO and the blends containing 10 and 20% PVAc resulting from the swelling of IL regions that sucks in PVAc whereas the segregation distance is increased for the blend containing 30% PVAc resulting from the expulsion of PVAc from IL regions during depressurizing of CO_2. Comparing Figs. 5 and 7, the lamellar size distribution appears to be broader and the lamellar stacks more disorganized for the samples after CO_2 treatments because the first minimum and the first maximum of the one-dimensional correlation function appear to be broader after CO_2 treatments.

4. Conclusions

The phase structure of crystalline/amorphous PEO/PVAc blends could be considerably affected upon CO_2 treatment as demonstrated by the drastic increase of SAXS intensity due to the enhancement of electron density contrast between the crystalline and amorphous layers in the lamellar stacks. The effects of CO_2 treatment on the blends involved the followings: (1) the amorphous PEO in the IL regions was swollen, (2) the PVAc might be expelled from the IL regions, (3) the thickness of the crystal and amorphous layer in the lamellar stacks were both increased, (4) the distance of segregation for neat PEO and PEO-rich blends was decreased, (5) the lamellar size distribution was widened, (6) the lamellar stacks were disorganized.

Acknowledgements

We thank National Science Council of Republic of China for financial support for this work. We are also grateful for Prof. Tsang-Lang Lin of the Department of Engineering and System Science at National Tsing Hua University for assistance in SAXS measurements.

References

[1] Stein RS, Khambatta FB, Warner FP, Russell T, Escala A, Balizer E. J Polym Symp 1978;63:313.
[2] Chen HL, Li LJ, Lin TL. Macromolecules 1998;31:2255.
[3] Defieuw G, Groeninckx G, Reynaers H. Polym Commun 1989;30:267.
[4] Defieuw G, Groeninckx G, Reynaers H. Polymer 1989;30:595.
[5] Hudson SD, Davis DD, Lovinger AJ. Macromolecules 1992;25:1759.
[6] Huo PP, Cebe P, Capel M. Macromolecules 1993;126:4275.
[7] Sauer BB, Hsiao BS. J Polym Sci, Polym Phys Ed 1993;31:901.
[8] Keith HD, Padden FJ. J Appl Phys 1975;35:1270.
[9] Kalfoglou NK. J Polym Sci, Polym Phys Ed 1982;20:1295.
[10] Munoz E, Calahorra M, Santamaria A. Polym Bull 1982;7:295.
[11] Martuscelli E, Silvestre C, Gismondi C. Markromol Chem 1985;186:2161.
[12] Silvestre C, Karasz FE, Macknight WJ, Martuscelli E. Eur Polym J 1987;23:745.
[13] Chen X, Hu H, Yin J, Zheng C. J Appl Polym Sci 1995;56:247.
[14] Chen X, An L, Li L, Yin J, Sun Z. Macromolecules 1999;32:5905.
[15] Hamada F, Shiomi T, Fujisawa K, Nakajima A. Macromolecules 1980;13:729.
[16] Natansohn A. J Polym Sci, Polym Phys Ed 1995;23:305.
[17] Martuscelli E, Canetti M, Vicini L, Seves A. Polymer 1982;23:331.
[18] Talibuddin S, Wu L, Runt J, Lin JS. Macromolecules 1996;29:7527.
[19] Chiu H-J, Chen H-L, Lin JS. Polymer 2001;42:5749.
[20] Chen H-L, Wang S-F. Polymer 2000;41:5157.
[21] Chen H-L, Liu HH, Lin J-S. Macromolecules 2000;33:4856.
[22] Chiu H-J, Chen H-L, Lin T-L, Lin JS. Macromolecules 1999;32:4969.
[23] Chen H-L, Wang S-F, Lin T-L. Macromolecules 1998;31:8924.
[24] Chen H-L, Li L-J, Lin T-L. Macromolecules 1998;31:2255.
[25] Wenig W, Karasz FE, MacKnight WJ. J Appl Phys 1975;46:4194.
[26] Khambatta FB, Warner F, Rusell TP, Stein RS. J Polym Sci, Polym Phys Ed 1976;14:1391.
[27] Russell TP, Stein RS. J Polym Sci, Polym Phys Ed 1983;21:999.
[28] Goel SK, Beckman EJ. Polym Engng Sci 1994;34:1137.
[29] Goel SK, Beckman EJ. Polym Engng Sci 1994;34:1148.
[30] Arora KA, Lesser AJ, McCarthy TJ. Polym Engng Sci 1998;38:2055.
[31] Stafford CM, Russell TP, McCarthy TJ. Macromolecules 1999;32:7610.
[32] Lee M, Tzoganakis C, Park CB. Polym Engng Sci 1998;38:1112.
[33] Elkovitch MD, Tomasko DL, Lee LJ. Polym Engng Sci 1999;39:2075.
[34] Yeo S-D, Kiran E. Macromolecules 1999;32:7325.
[35] Elkovitch MD, Lee LJ, Tomasko DL. Polym Engng Sci 2000;40:1850.
[36] Chiou JS, Barlow JW, Paul DR. J Appl Polym Sci 1985;30:3911.
[37] Beckman E, Porter RS. J Polym Sci, Part B: Polym Phys 1987;25:1511.
[38] Gross SM, Roberts GW, Kiserow DJ, DeSimone JM. Macromolecules 2000;33:40.
[39] Strobl GR, Schneider M. J Polym Sci, Polym Phys Ed 1980;18:1343.
[40] Vidotto G, Levy DL, Kovacs A. J Kolloid Z Z Polym 1968;230:299.
[41] Kazarian SG, Vincent MF, Bright FV, Liotta CL, Eckert CA. J Am Chem Soc 1996;118:1729.
[42] Kortleve G, Vonk VG. Kolloid-Z 1967;220:19.
[43] Kortleve G, Vonk VG. Kolloid-Z 1968;225:124.
[44] Debye P, Bueche AM. J Appl Phys 1949;20:518.
[45] Debye P, Anderson Jr HR, Brumberger H. J Appl Phys 1957;28:679.
[46] Ruland WJ. J Appl Crystallogr 1971;4:70.
[47] Zhang Z, Handa YP. Macromolecules 1997;30:8505.
[48] Hoffman JD, Weeks JJ. J Res Natl Bur Stand A: Phys Chem 1962;66A:13.
[49] Hoffman JD, Miller RL. Polymer 1997;38:3151.